Motion Compensation for Accurate Position Estimation of Ground Moving Targets using the Multi-Channel Airborne System DBFSAR

André Barros Cardoso da Silva, Sushil Kumar Joshi and Stefan Valentin Baumgartner
Microwaves and Radar Institute, German Aerospace Center (DLR), Oberpfaffenhofen, Germany
Email: andre.silva@dlr.de

Abstract

The accurate estimation of the target's position on the ground is a crucial step for air-based surveillance systems. For the particular case of radar systems with multiple receive channels, the target's position on the ground can be accurately obtained after estimating its direction-of-arrival (DOA) angle. The problem is that, in practice, the aircraft's motion tilts the antenna array and introduces undesired phase differences among the receive channels. Consequently, the DOA angle estimation accuracy can be severely impacted. This paper presents a fast and robust algorithm for correcting the undesired phases differences introduced by the aircraft's motion among the multiple receive channels. The proposed algorithm is tested and validated using simulated radar data as well as radar data acquired with the DLR's new multi-channel airborne system digital beamforming SAR (DBFSAR).

1 Introduction

Airborne radars present the advantage of acquiring the data independently from the daylight and weather conditions, which makes such radars very attractive for surveillance applications. A very important requirement for air-based surveillance systems is the accurate estimation of the target's position on the ground. In particular, if the airborne radar system is equipped with an antenna array with multiple receive (Rx) channels, then the target position on the ground can be accurately obtained after estimating its direction-of-arrival (DOA) angle [1][2].

The DOA angle of the target must be measured with respect to the azimuth or flight direction, which is depicted by the blue axis in **Figure 1**. The problem in practice is that atmospheric turbulences cause variations in the aircraft's attitude angles (yaw, pitch and roll) and such variations tilt (or squint) the antenna array axis [3], as depicted by the red axis in **Figure 1**. The variation of the attitude angles introduces an additional across-track baseline component among the multiple Rx channels, which can cause range dependent phases as well as DOA angle variations. The correction of such undesired phases eliminates the additional across-track baseline component, so that only the along-track baseline component remains. In other words, after correcting the undesired interferometric phases, the antenna array axis becomes aligned with the aircraft's azimuth axis, and thus the DOA angle of the target can be accurately estimated.

A calibration algorithm is proposed in [4] for moving target indication (MTI) applications, in which an important step is the estimation of the interferometric phase offsets among the multiple Rx channels. Although the calibration is accurate, the phase offsets are not adaptively estimated, and therefore this algorithm is found robust only in case of low squint angle acquisitions and moderately flat terrains.

Another calibration algorithm is proposed in [5] with the aim to compensate the undesired phases among the Rx channels. Although this algorithm deals effectively with high squint angle acquisitions and high terrain's topographic variations, the achieved position accuracy of the target is found to be poor since only two Rx channels are used. In addition, the algorithm presented in [5] requires high computational power since it operates only with fully focused synthetic aperture radar (SAR) images, which makes this algorithm principally unsuitable for real-time applications.

This paper presents a fast and robust phase correction algorithm that is applicable for high squint angle acquisitions as well as high terrain's topographic variations. For correcting the interferometric phases among the Rx channels, the proposed algorithm requires the precise geographical positions of all bistatic phase centers of the Rx antennas, which are generally provided by the aircraft's navigation system and the known lever arms. It also requires the elevation of the terrain, which can be obtained from a digital elevation model (DEM). The proposed algorithm operates on range-compressed radar data and does not require the time-consuming SAR processing. Thus, it is principally suitable for real-time applications.

The applicability of the proposed algorithm and its performance are validated using simulated radar data as well as X-band radar data sets acquired with the DLR's new multi-channel airborne system digital beamforming SAR (DBFSAR) [6].

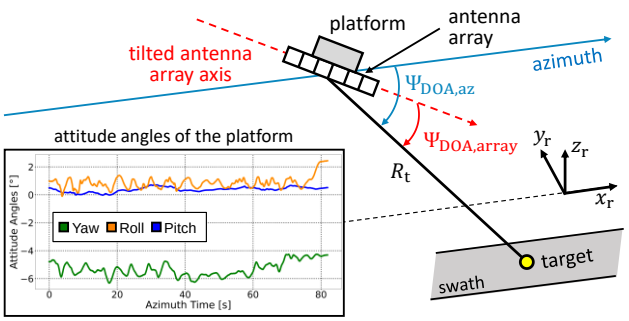

Figure 1: Acquisition geometry showing the problem of a tilted antenna array on the target's DOA angle estimation. The radar coordinate system projected on the ground is given by $[x_r, y_r, z_r]$, where x_r coincides with the azimuth direction.

2 DOA Angle and Position Estimation

The multi-channel signal model can be expressed by [7]:

$$\boldsymbol{s}(t) = a_\mathrm{s} e^{-j\frac{4\pi}{\lambda}R_\mathrm{t}(t)} \begin{bmatrix} D_\mathrm{tx}\left[u_\mathrm{array}(t)\right] D_\mathrm{rx,1}\left[u_\mathrm{array}(t)\right] e^{j\frac{2\pi}{\lambda}u_\mathrm{array}(t)x_1} \\ \vdots \\ D_\mathrm{tx}\left[u_\mathrm{array}(t)\right] D_\mathrm{rx,M}\left[u_\mathrm{array}(t)\right] e^{j\frac{2\pi}{\lambda}u_\mathrm{array}(t)x_\mathrm{M}} \end{bmatrix} = a_\mathrm{s} e^{-j\frac{4\pi}{\lambda}R_\mathrm{t}(t)} \boldsymbol{d}\left[u_\mathrm{array}(t)\right] \quad (1)$$

where a_s is the reflectivity of the scatterer, λ is the radar wavelength, M is the number of Rx channels, R_t is the slant range of the target, D_tx and $D_\mathrm{rx,m}$ are the complex transmit and receive azimuth antenna characteristics of the m-th channel, respectively, and x_m is the position of the antenna phase center in the azimuth direction with respect to the antenna array's center (cf. **Figure 2**). The term $\boldsymbol{d}$ is known as beamforming or DOA vector, u_array is the directional cosine with respect to the antenna's array axis and t is the azimuth time.

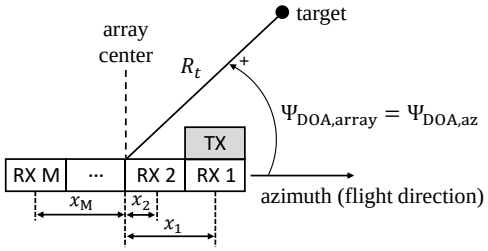

Figure 2: Acquisition geometry considering a multi-channel antenna and zero squint angle (i.e., the antenna array axis is perfectly aligned with the azimuth direction).

The beamforming vector $\boldsymbol{d}$ is used for estimating the target's directional cosine according to the maximum likelihood estimator [8]:

$$\hat{u}_\mathrm{array} = \underset{u_\mathrm{array}}{\mathrm{argmax}} \left\{ \left| \boldsymbol{d}^H\left(u_\mathrm{array}, f_\mathrm{a}\right) \widehat{\boldsymbol{R}}_\mathrm{W}^{-1}(f_\mathrm{a}) \boldsymbol{Z}(r_\mathrm{k}, f_\mathrm{a}) \right|^2 \right\} \quad (2)$$

where $[\cdot]^H$ denotes the Hermitian operator (complex conjugate transposition), f_a denotes the Doppler bin, r_k denotes the slant range to bin k, and $\boldsymbol{Z}$ denotes the multi-channel data in range-Doppler domain. The term $\widehat{\boldsymbol{R}}_\mathrm{W}$ is the clutter covariance matrix, which can be estimated adaptively from the radar data in order to perform clutter suppression (cf. some strategies proposed in [9]).

For applications in which high signal-to-clutter plus noise ratios (SCNR) are expected, the moving targets can be detected in the range-Doppler domain without clutter suppression. In such cases, the term $\widehat{\boldsymbol{R}}_\mathrm{W}$ can be omitted in (2), so that the maximum likelihood estimator becomes:

$$\hat{u}_\mathrm{array} = \underset{u_\mathrm{array}}{\mathrm{argmax}} \left\{ \left| \boldsymbol{d}^H\left(u_\mathrm{array}, f_\mathrm{a}\right) \boldsymbol{Z}(r_\mathrm{k}, f_\mathrm{a}) \right|^2 \right\}. \quad (3)$$

The target's DOA angle with respect to the antenna array axis is obtained according to: $\widehat{\Psi}_\mathrm{DOA,array} = \cos^{-1}\left(\hat{u}_\mathrm{array}\right)$.

For estimating the target's position on the ground, consider the acquisition geometry in the local Cartesian coordinate system $[\tilde{x}, \tilde{y}, \tilde{z}]$ shown in **Figure 3**. In this figure, α_p is the platform's course angle with respect to the $\tilde{x}$ (Easting) axis. The terms Δx_r and Δy_r (in red) are the distances on ground (in radar coordinates) between the target and the platform positions, which are obtained as:

$$\Delta x_\mathrm{r} = R_\mathrm{t} \cdot \cos\left(\widehat{\Psi}_\mathrm{DOA,az}\right) \quad (4)$$

$$\Delta y_\mathrm{r} = \sqrt{\left(R_\mathrm{t} \cdot \sin\left(\widehat{\Psi}_\mathrm{DOA,az}\right)\right)^2 - \left(\tilde{z}_\mathrm{p1} - \tilde{z}_t\right)^2} \quad (5)$$

where $\widehat{\Psi}_\mathrm{DOA,az}$ denotes the target's DOA angle with respect to the azimuth direction, $\tilde{z}_\mathrm{p1}$ denotes the flight altitude from the reference channel Rx1 and $\tilde{z}_\mathrm{t}$ denotes the terrain's elevation obtained from a DEM. It is important to mention that after applying the proposed phase correction algorithm (cf. Section 3), the antenna array axis becomes perfectly aligned with the azimuth or flight direction, and therefore $\widehat{\Psi}_\mathrm{DOA,array} = \widehat{\Psi}_\mathrm{DOA,az}$ (cf. also **Figure 2**).

The target' position on the ground in local coordinates $\tilde{\boldsymbol{x}}_\mathrm{t}$ is calculated according to (cf. **Figure 3**):

$$\tilde{\boldsymbol{x}}_\mathrm{t} = \tilde{\boldsymbol{p}}_1 + \Delta x_\mathrm{r} \cdot \vec{e}_{\tilde{x}} + \Delta y_\mathrm{r} \cdot \vec{e}_{\tilde{y}} - h_\mathrm{t} \cdot \vec{e}_{\tilde{z}} \quad (6)$$

where $\tilde{\boldsymbol{p}}_1$ is the platform's position in the local coordinates obtained from the reference channel Rx1 and $h_\mathrm{t} = \tilde{z}_\mathrm{p1} - \tilde{z}_t$ is the height difference between the first antenna element and the target.

The unit vectors in (6) are defined according to:

$$\vec{e}_{\tilde{x}} = \left[\cos(\alpha_\mathrm{p}), \sin(\alpha_\mathrm{p}), 0\right]^\mathrm{T} \quad (7)$$

$$\vec{e}_{\tilde{y}} = \left[A \cdot \sin(\alpha_\mathrm{p}), -A \cdot \cos(\alpha_\mathrm{p}), 0\right]^\mathrm{T} \quad (8)$$

$$\vec{e}_{\tilde{z}} = [0, 0, 1]^\mathrm{T} \quad (9)$$

where $[\cdot]^\mathrm{T}$ denotes the transpose operator.

In (8), it is assumed $A = 1$ for a right-looking antenna (as in the case of the DBFSAR system [6]) and $A = -1$ for a left-looking antenna.

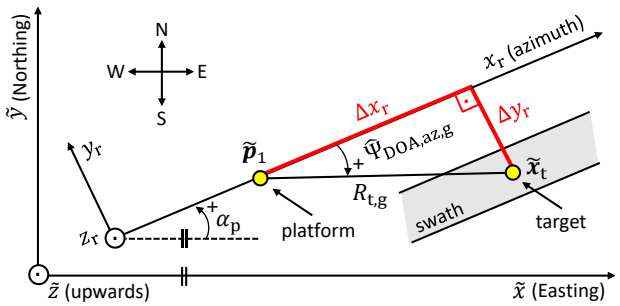

Figure 3: Acquisition geometry used for the calculation of the target's position on the ground in local coordinates $[\tilde{x}, \tilde{y}, \tilde{z}]$. The terms $\widehat{\Psi}_\mathrm{DOA,az,g}$ and $R_\mathrm{t,g}$ are the ground projections of the terms $\widehat{\Psi}_\mathrm{DOA,az}$ and R_t, respectively.

3 Proposed Algorithm

The principles of the proposed algorithm can be explained based on the acquisition geometry shown in **Figure 3**, where the radar system is equipped with multiple Rx channels and the antenna array axis is tilted due to the platform motion (yaw, pitch and roll).

The proposed phase correction algorithm is carried out in three main steps. In the first step, the original Rx channel positions $\tilde{\boldsymbol{p}}_m$ are mapped onto the linearized reference track of channel Rx1 by means of vector orthogonal projection (cf. Section 3.1 and the detail box in **Figure 4**).

In the second step, the reference points on the ground $\tilde{\boldsymbol{g}}_m$ are calculated for each Rx channel m by using the coordinates of the relocated Rx channel positions $\tilde{\boldsymbol{p}}'_m$ (cf. Section 3.2).

The range displacements $R_m - R_\mathrm{t}$ are calculated in the last step. Such slant range differences are directly related to the phase shifts to be compensated for each Rx channel m (cf. Section 3.3).

It is pointed out that no phase correction is required for the reference channel Rx1, since the slant range difference in this case is zero.

3.1 Relocation of Receive Channel Positions

The mapping of the original Rx channel positions $\tilde{\boldsymbol{p}}_m$ onto the reference track (e.g., from channel Rx1) is carried out according to the following main steps:

i. Obtain the original bistatic antenna phase center positions of all Rx channels at the n-th transmitted pulse: $\tilde{\boldsymbol{p}}_m[n]$. Additionally, obtain the original position of the reference channel Rx1 at a subsequent transmitted pulse: $\tilde{\boldsymbol{p}}_1[n+1]$.

ii. Calculate the reference vector along the azimuth or flight direction by using the reference channel Rx 1 (cf. black vector in **Figure 4**):

$$\tilde{\boldsymbol{b}}_\mathrm{az} = \tilde{\boldsymbol{p}}_1[n+1] - \tilde{\boldsymbol{p}}_1[n] \,. \tag{10}$$

iii. Obtain the vectors corresponding to all original Rx channel positions (cf. orange vector in **Figure 4**):

$$\tilde{\boldsymbol{a}}_m = \tilde{\boldsymbol{p}}_m[n] - \tilde{\boldsymbol{p}}_1[n] \,. \tag{11}$$

iv. Perform the orthogonal projection of the vector $\tilde{\boldsymbol{a}}_m$ onto the reference vector $\tilde{\boldsymbol{b}}_\mathrm{az}$ (cf. green vector in **Figure 4**):

$$\mathrm{proj}_{\tilde{\boldsymbol{b}}_\mathrm{az}}\, \tilde{\boldsymbol{a}}_m = \left(\frac{\tilde{\boldsymbol{a}}_m \cdot \tilde{\boldsymbol{b}}_\mathrm{az}}{\tilde{\boldsymbol{b}}_\mathrm{az} \cdot \tilde{\boldsymbol{b}}_\mathrm{az}}\right) \tilde{\boldsymbol{b}}_\mathrm{az} \,. \tag{12}$$

v. Obtain the relocated Rx channel positions $\tilde{\boldsymbol{p}}'_m$ onto the reference track of channel Rx1 according to:

$$\tilde{\boldsymbol{p}}'_m[n] = \tilde{\boldsymbol{p}}_1[n] + \mathrm{proj}_{\tilde{\boldsymbol{b}}_\mathrm{az}}\, \tilde{\boldsymbol{a}}_m \,. \tag{13}$$

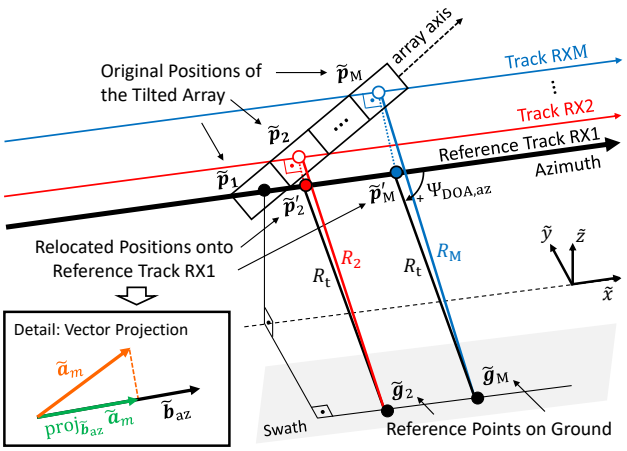

Figure 4: Acquisition geometry showing the main steps of the proposed algorithm. The figure is shown for a specific transmitted pulse n and at a certain slant range bin k. For simplicity, $\alpha_\mathrm{p} = 0°$ is considered (cf. also **Figure 3**).

3.2 Calculation of Reference Point Positions on the Ground

The coordinates of the reference points on the ground at the slant range bin k are obtained by:

$$\tilde{\boldsymbol{g}}_m[k] = \tilde{\boldsymbol{p}}'_m + \Delta x_\mathrm{r}[k] \cdot \vec{e}_{\tilde{x}} + \Delta y_\mathrm{r}[k] \cdot \vec{e}_{\tilde{y}} - h \cdot \vec{e}_{\tilde{z}} \,. \tag{14}$$

As it can be seen in (14), the relocated Rx channel positions $\tilde{\boldsymbol{p}}'_m$ are used for calculating the reference point positions on the ground. Moreover, it is pointed out that the terms Δx_r and Δy_r are obtained with (4)-(5) by setting the DOA angle to the broadside direction (i.e., $\Psi_\mathrm{DOA,az} = 90°$) and by using the slant ranges $R_\mathrm{t}[k]$ (cf. **Figure 4**).

3.3 Slant Range Differences and Phase Correction

The slant ranges R_m between the original Rx positions $\tilde{\boldsymbol{p}}_m$ and their respective reference points on the ground $\tilde{\boldsymbol{g}}_m$ are obtained for each slant range bin k according to:

$$R_m[k] = \sqrt{\left(\tilde{x}_\mathrm{pm} - \tilde{x}_\mathrm{gm}\right)^2 + \left(\tilde{y}_\mathrm{pm} - \tilde{y}_\mathrm{gm}\right)^2 + \left(\tilde{z}_\mathrm{pm} - \tilde{z}_\mathrm{t}\right)^2} \,. \tag{15}$$

The slant range differences are computed by

$$\Delta R_m[k] = R_m[k] - R_\mathrm{t}[k] \tag{16}$$

and the phases to be corrected for each Rx channel are:

$$\emptyset_m[k] = \exp\left\{j \frac{4\pi}{\lambda} \cdot \Delta R_m[k]\right\} \,. \tag{17}$$

In the results shown in this paper, the proposed algorithm is applied to all slant range bins of the radar data. However, it has to be mentioned that in case the moving targets are detected a priori, the phase correction can then be applied directly to the slant range bins of the detected targets. Thus, the overall processing time can be even further reduced.

4 Theoretical Evaluation

The performance of the proposed phase correction algorithm is evaluated in this section by using simulated multi-channel radar data. The simplified flowchart of the simulation framework is shown in **Figure 5**.

Three inputs are required for generating the simulated multi-channel radar data: 1) the target's true position on the ground, which is set by the user; 2) the radar and the acquisition geometry parameters, which are listed in **Table 1**; and 3) the tracks of all Rx channels. These tracks include in their computation the platform's attitude angles (yaw, pitch and roll), as shown in the detail box of **Figure 1**.

By using the tracks of the Rx channels and the target's position on the ground, the range histories and the azimuth signals of the target can be obtained for all Rx channels.

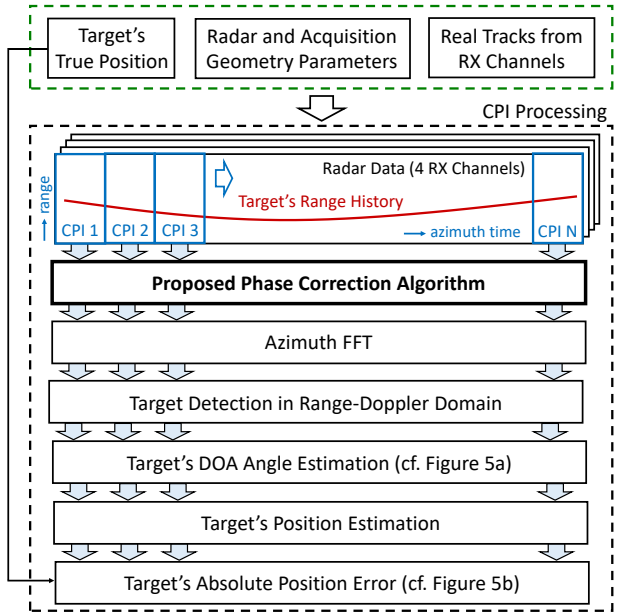

Figure 5: Simplified flowchart used for assessing the performance of the proposed phase correction algorithm.

The simulated multi-channel data are initially segmented into *N* small coherent processing intervals (CPIs) along the azimuth direction. Then, the phase correction is applied to all range bins contained in a CPI. Next, the CPIs are transformed into range-Doppler domain via azimuth FFT (fast Fourier transform).

The target detection is carried out in range-Doppler domain. After detection, the target's slant range and Doppler frequency are measured. The DOA angle of the target is estimated via beamforming with (3) and then its position on the ground is computed with (4)-(9). Finally, the target's absolute position error is obtained by calculating the absolute difference between its true and estimated positions.

Figure 6a shows a comparison between the target's DOA angles obtained with and without the proposed phase correction algorithm. It can be clearly seen that the estimated DOA angles without phase correction (red) not only fluctuate over time but also present a root mean square error (RMSE) of about 2.2°. This error in the DOA angle estimates lead to an absolute position error of about 106 m, as shown in **Figure 6b** (red).

On the other hand, after applying the proposed phase correction algorithm the estimated DOA angles overlap very well with the true DOA angles (magenta dotted line in **Figure 6a**) and give a mean DOA and position errors of nearly 0° and 0.3 m, respectively (cf. blue curves in **Figure 6**).

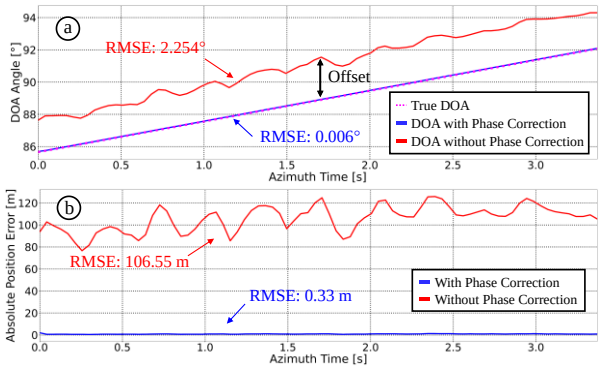

Figure 6: Simulation results with and without phase correction: (a) target's DOA angle; (b) absolute position error.

5 Experimental Results

The proposed phase correction algorithm is tested in this section using X-band VV-polarized airborne radar data sets. The flight campaign with the DLR's new airborne system DBFSAR [6] was conducted in October 2020 over the Lake Ammersee, in Germany. **Table 1** summarizes the main radar and acquisition geometry parameters.

Figure 7 (top) shows the Google Earth image of the test site, which is overlaid with fully focused SAR images only for visualization purposes. Five electrical boats #1-5 (size ≈ 3.5 m x 1.5 m) and a sailboat #6 (size ≈ 5.0 m x 2.0 m) were located in the region of interest (ROI). The boats #1-4 moved in different linear tracks, boat #5 moved in circles and the sailboat #6 moved freely within the ROI. The absolute ground velocities of the boats were in the order of 1.5 m/s and their tracks were recorded by handheld GPS devices (cf. the GPS tracks in **Figure 7** bottom).

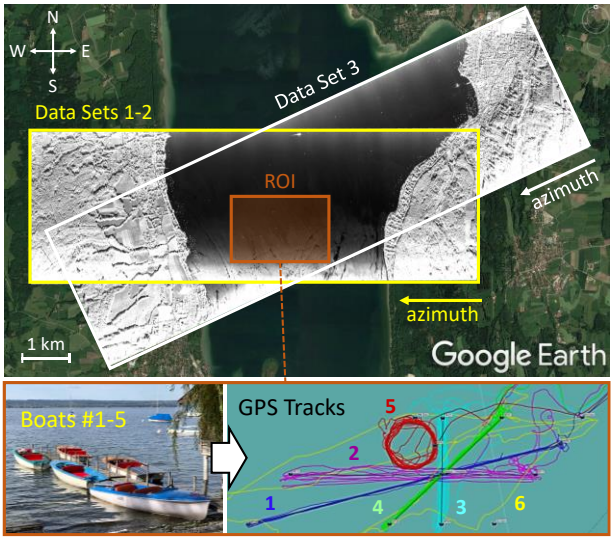

Figure 7: Test site in the region of the Lake Ammersee, where six boats moved within the ROI (orange box). Data sets 1 and 2 were acquired with the same flight direction.

5.1 Accuracy of Estimated DOA Angles

In this section, the accuracy of the estimated DOA angles is evaluated with and without applying the proposed phase correction algorithm in the data set 1 (cf. **Figure 7**).

It can be seen from **Figure 8a** that the DOA angles estimated without phase correction change significantly due to the platform motion. An example is shown in **Figure 8c**, where the red histogram shows the high variation of the estimated DOA angles within the ROI without phase correction.

In contrast, **Figure 8b** shows the great improvement of the estimated DOA angles achieved after correcting the undesired phases. Note that in this figure the DOA angle scale spams from 89.5° to 90.5°. This narrow scale allows, for instance, to observe in detail the variation of the DOA angle estimates especially in the regions of land (i.e., outside the ROI). This DOA angle variation is caused by the terrain's topographic variation, since the phase correction was carried out in this case for the entire data set by using the mean terrain's elevation of the ROI (cf. **Table 1**) instead of a DEM, for simplicity.

The blue histogram in **Figure 8c** shows that, after phase correction, the mean estimated DOA angle within the ROI is $\bar{\Psi}_{\mathrm{DOA,array}} = 89.74°$, which leads to an offset of $\Psi_{\mathrm{DOA,offset}} = 0.26°$ with respect to the reference value of $\Psi_{\mathrm{DOA,array}} = 90°$ (dashed green line). This offset is mainly caused by the surface velocity of the lake in the line-of-sight direction of the radar [10]. The lake's surface velocity can be principally estimated as function of the $\Psi_{\mathrm{DOA,offset}}$. However, this computation is out of the scope of this paper.

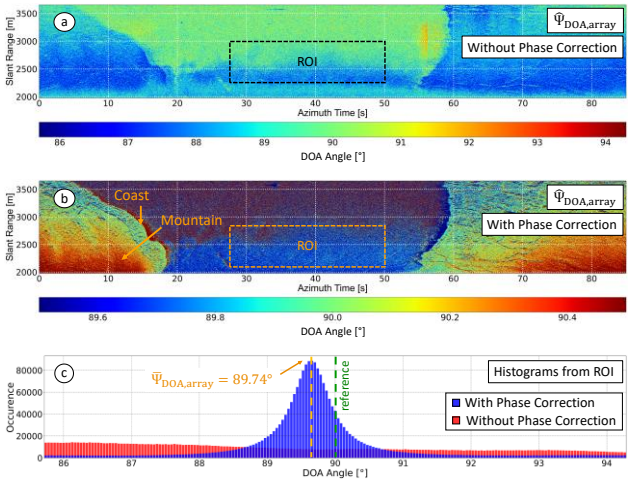

Figure 8: DOA angles estimated from data set 1: (a) without and (b) with phase correction. The histograms of the DOA angles estimated within the ROI are shown in (c).

5.2 Accuracy of Estimated Positions

The moving boats need to be detected and tracked before evaluating their position estimation accuracy. For the results presented in this section, the detection and tracking were carried out by using the algorithms proposed in [11] [12]. Besides, it is pointed out that no clutter suppression was performed and single-channel data were used for detecting the moving boats. Naturally, there is no restriction for using multi-channel data for detection, in which either sum-channel data or clutter suppressed data could be used.

Quantity	Value
Velocity of the platform	90 m/s
Number of Tx/Rx channels	1/6
Pulse repetition frequency (PRF)	3004 Hz
Slant range resolution	0.3 m
Effective along-track baseline	0.1 m
Wavelength	0.03155 m
Maximum squint angle	5°
Mean altitude of the platform (above ellipsoid)	2498 m
Mean terrain's height of the ROI (above ellipsoid)	579 m

Table 1: Main radar and acquisition geometry parameters for data sets 1 to 3.

Data Set	Boat (#)	Absolute Position Error [m] **Without Correction**	Absolute Position Error [m] **With Correction**	SCNR [dB]
1	1	180.34	17.21	17.40
	2	185.41	16.62	16.43
	3	174.87	10.42	15.96
	5	186.91	10.21	15.29
	6	175.83	9.72	18.63
2	1	179.48	9.67	19.27
	2	176.24	15.84	17.95
	4	178.78	10.19	16.83
	5	175.79	14.33	14.27
	6	176.86	10.31	19.11
3	1	252.54	19.16	17.12
	2	252.53	10.21	15.71
	3	127.91	7.63	13.71
	4	250.87	10.39	19.44
	5	262.53	13.38	14.15
	6	129.22	9.31	22.61

Table 2: SCNR and position errors of the detected boats in data sets 1 to 3.

Figure 9 shows the geocoded radar detections (orange) obtained from the moving boats within the ROI in data set 1, before and after the phase correction. The GPS tracks (white) are shown for the entire flight duration (≅ 85 s) and the arrows indicate the direction of motion of the boats.

In **Figure 9a**, it can be seen that without applying the phase correction algorithm the geocoded radar detections of the boats are significantly displaced from their GPS tracks. In contrast, after applying the phase correction algorithm, the geocoded radar detections are found very close to their corresponding GPS tracks, as shown in **Figure 9b**. It is pointed out that the boat #4 could not be detected in data set 1 due to its low SCNR.

As an example, **Figure 10** shows the SCNR values and the absolute position errors obtained from boat #1 after phase correction in data set 1. In this example, an average SCNR of 17.40 dB and a position error (RMSE) of 17.21 m were obtained. Such measurements were carried out for all detected boats within the ROI of data sets 1 to 3. The results are summarized in **Table 2**.

In **Table 2**, it can be seen that without phase correction the absolute position errors were found higher than 175 m for data sets 1 and 2, and they reached up to 262 m for data set 3, which had the highest squint angle in the order of 5°.

In contrast, after correcting the phases the absolute position errors of the boats have significantly decreased to less than 20 m. Such a position estimation accuracy is considered very good for airborne radar-based moving target monitoring, especially because in this experiment small boats and strongly changing aircraft attitude angles were taken into account.

Finally, it is pointed out that further details and discussions about the experimental results obtained with the proposed phase correction algorithm can be found in [13].

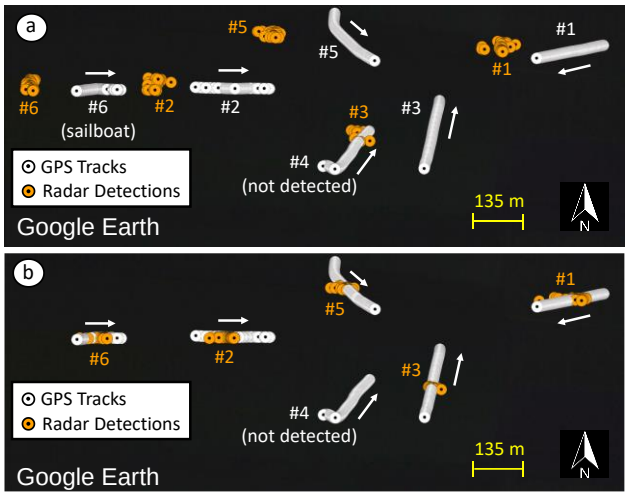

Figure 9: Geocoded radar detections (orange) of the moving boats obtained within the ROI of data set 1: (a) before and (b) after phase correction. The GPS tracks of the boats (white) as well as their moving directions are also shown.

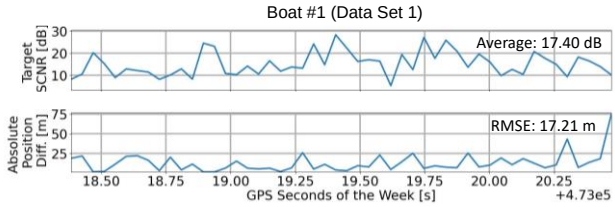

Figure 10: Target's SCNR and absolute position errors obtained from boat #1 in data set 1 after phase correction.

6 Conclusion

This paper presents a fast and robust phase correction algorithm for ground moving target monitoring applications using multi-channel airborne radar data. The experimental results show that the proposed algorithm is able to correct the undesired interferometric phases among the multiple receive channels effectively, so that the absolute position errors of the moving boats were better than 20 m. Such position accuracy is considered very good, especially taking into account that the detectability of the small boats was very low and the radar data sets were acquired with high squint angles that reached up to 5°.

7 Literature

[1] W. L. Melvin, "A STAP overview," *IEEE Aerospace and Electronic Systems Magazine*, vol. 19, no. 1, pp. 19–35, Jan. 2004.

[2] J. R. Guerci, *Space-Time Adaptive Processing for Radar*, 1st ed., no. 1, Norwood, MA, USA: Artech House, 2003.

[3] G. K. Borsari, "Mitigating effects on STAP processing caused by an inclined array", *IEEE Radar Conference*, pp. 135-140, 1998.

[4] A. B. C. Silva, S. V. Baumgartner, F. Q. de Almeida, and G. Krieger, "In-Flight Multichannel Calibration for Along-Track Interferometric Airborne Radar," *IEEE Transactions on Geoscience and Remote Sensing*, vol. 59, no. 4, pp. 3104-3121, Apr. 2021.

[5] L. Yang, T. Wang, and Z. Bao, "Ground Moving Target Indication Using an InSAR System With a Hybrid Baseline," *IEEE Geoscience and Remote Sensing Letters*, vol. 5, no. 3, pp. 373–377, Jul. 2008.

[6] A. Reigber, E. Schreiber, K. Trappschuh, S. Pasch, G. Müller, D. Kirchner, D. Geßwein, S. Schewe, A. Nottensteiner, M. Limbach, A. Schreiber, T. Rommel, R. Horn, M. Jäger, R. Scheiber, S. V. Baumgartner, S. K. Joshi, A. B. C. Silva, and A. Moreira, "The High-Resolution Digital-Beamforming Airborne SAR System DBFSAR," *Remote Sensing*, vol. 12, no. 11, pp. 1710, May 2020.

[7] J. H. G. Ender, C. H. Gierull, and D. Cerutti-Maori, "Improved space-based moving target indication via alternate transmission and receiver switching," *IEEE Transactions on Geoscience and Remote Sensing*, vol. 46, no. 12, pp. 3960-3974, Dec. 2008.

[8] F. C. Robey, D. R. Fuhrmann, E. J. Kelly, and R. Nitzberg, "A CFAR Adaptive Matched Filter Detector," *IEEE Transactions on Aerospace and Electronic Systems*, vol. 28, no. 1, pp. 208–216, Jan. 1992.

[9] A. B. C. Silva, S. V. Baumgartner, and G. Krieger, "Training Data Selection and Update for Airborne Post-Doppler STAP," *IEEE Transactions on Geoscience and Remote Sensing*, vol. 57, no. 8, pp. 5626–5641, Aug. 2019.

[10] A. Elyouncha, L. E. B. Eriksson, R. Romeiser and L. M. H. Ulander, "Measurements of Sea Surface Currents in the Baltic Sea Region Using Spaceborne Along-Track InSAR," *IEEE Transactions on Geoscience and Remote Sensing*, vol. 57, no. 11, pp. 8584-8599, Nov. 2019.

[11] S. K. Joshi, S. V. Baumgartner, A. B. C. Silva, and G. Krieger, "Range-Doppler Based CFAR Ship Detection with Automatic Training Data Selection," *Remote Sensing*, vol. 11, no. 11, p. 1270, May 2019.

[12] S. K. Joshi, S. V. Baumgartner, and G. Krieger, "Tracking and Track Management of Extended Targets in Range-Doppler Using Range-Compressed Airborne Radar Data," *IEEE Transactions on Geoscience and Remote Sensing*, June 2021 (early access).

[13] A. B. C. da Silva, S. K. Joshi, S. V. Baumgartner, F. Q. de Almeida, and G. Krieger, "Phase Correction for Accurate DOA Angle and Position Estimation of Ground-Moving Targets Using Multi-Channel Airborne Radar," *IEEE Geoscience and Remote Sensing Letters*, vol. 19, pp. 1–5, Jan. 2022.